53. S. Hammer, *Geophysics* **4**, 184 (1939).
54. R. J. Kirkpatrick, in *Initial Reports of the Deep Sea Drilling Project*, L. Dmitriev *et al.*, Eds. (Government Printing Office, Washington, D.C., 1979), vol. 46, p. 401.
55. R. L. Larson, *Scripps Inst. Oceanogr. Ref. 70-2* (1970).
46. R. L. Parker and S. P. Huestis, *J. Geophys. Res.* **79**, 1587 (1974).
57. T. M. Atwater and K. C. Macdonald, *Eos* **59**, 1198 (1978).

58. We acknowledge the highly competent support provided by *Alvin*'s operators, led by pilots D. Foster, R. Hollis, and G. Ellis; the crews of R.V. *Lulu* (J. Boord, master), R.V. *Melville* (A. Arsenault, master), and R.V. *New Horizon* (A. Phinney, master); and the members of the several hardworking scientific parties. F. Grassle and J. Kerridge made substantial contributions through analyses and descriptions of biological and mineralogical samples. L. Shure aided in the collection and analysis of the magnetic data. The expedition was funded by the Seabed Assessment Program of the National Science Foundation International Decade of Ocean Exploration office under grants NSF/OCE 78-01664, 78-21082, and 79-09984. Funds for mineralogical and geochemical analyses were provided by a grant from the Academic Senate, University of California, San Diego. Support for the electrical measurements was provided by the National Science Foundation and the Office of Naval Research (Earth Physics Branch).

Sulfide Deposits from the East Pacific Rise Near 21°N

R. Hekinian, M. Fevrier, J. L. Bischoff, P. Picot, W. C. Shanks

Summary. Massive sulfide deposits were discovered from the diving saucer *Cyana* on the accreting plate boundary region of the East Pacific Rise near 21°N. The deposits form conical and tubular structures lying on a basaltic basement. Mineralogical and geochemical analyses showed two main types of intimately associated products: a polymetallic sulfide-rich material composed of pyrite and marcasite in association, zinc-rich phases, and copper-rich compounds, and an iron-rich oxide and hydroxide material (also called gossan) composed largely of goethite and limonite. Silicate phases such as opaline, silica, iron-silicon clay, and trace amounts of mica and zeolite are encountered in both types of material. Possible mechanisms for the formation of the sulfide deposits on the East Pacific Rise are discussed.

The early discoveries of hydrothermal products at accreting plate boundaries were sediments rich in iron and manganese (*1*). More recent findings of strongly fractionated iron-manganese concretions, material rich in silicon-iron clay, and hydrous iron oxides have been collected from the Galápagos spreading center (*2, 3*), from the Mid-Atlantic Ridge near 26°N (*4, 5*) and 37°N (*6*), and from the Gulf of Aden (*7*). Direct visual observations of thermal springs were made during a submersible study on the rift valley of the Galápagos spreading center (*8*).

The first discovery of a sizable submarine polymetallic sulfide deposit on a ridge system was made in the Red Sea during the international Indian Ocean expedition (1963 to 1965). In addition, many ancient massive sulfide deposits found in ophiolites are thought to have been formed on the sea floor in large oceans or marginal basins. These deposits consist primarily of pyrite, chalcopyrite, and sphalerite (*9–12*). The ophiolitic massive sulfide deposits, such as those in the Troodos complex in Cyprus (*13*), Semail in Oman (*14*), and Betts Cove and York Harbor in Newfoundland (*12, 15*), appear to represent ancient oceanic crust formed at mid-oceanic spreading ridges. A summary of the ophiolite complexes containing sizable ore deposits around the world is given by Coleman (*16*).

A recently formed massive sulfide deposit with similarities to the ophiolitic deposits was recently discovered by a manned submersible on the East Pacific Rise at 21°N during a French-American-Mexican joint project (project RITA) on rapidly spreading ridges (*17, 18*) (Fig. 1). The East Pacific Rise deposit occurs at a spreading ridge at 21°N. The rate of separation at the site, 3 centimeters a year, appears to have been constant during the last 4 million years (*18*). As indicated by deep-tow studies (*19*), the ridge crest in the area is dominated by a central zone of volcanic hills about 2 to 5 kilometers wide flanked on either side by a zone of open fissures.

More recent dives in the region by the submersible *Alvin* have discovered other massive sulfide mounds and actively discharging hydrothermal vents and solid particles with fluid temperatures of 375° ± 25°C (*20, 21*). Conical plumes discharging sulfide minerals on the sea floor were recently predicted by Solomon and Walshe (*22*) from experimental studies of deposits of the Cyrpus and Kuroko type. We present here the results of mineralogical and geochemical studies of sulfide deposits during dives of the submersible *Cyana* at 21°N (*23*).

Geologic Setting of the Sulfide Deposit

The deposits were sampled at two sites (Cy 78-08 and Cy 78-12) located on the flanks of steep-sided structural depressions about 20 to 30 meters deep and 20 to 30 meters wide, situated 700 to 800 meters west of the axis of the East Pacific Rise (Fig. 1) (*17*). The general area consists of a 1.5-km-wide band of fissured and faulted terrane associated with a horst and graben zone (*17, 24*). The massive sulfide deposits form roughly cylindrical hills ranging up to 10 m high and averaging 5 m in diameter (*23*). In an area visited during dive Cy 78-8, at least three vertical hills aligned in an approximately north-south direction (025°) were seen over a distance of about 50 m. The hills are about 3 to 4 m apart and the flanks of two different hills could be seen from the porthole of the submersible when it passed between them. The edifices are variegated with ocher, red, white, and dark gray colors and appear to be extremely porous. The first sample (8-14A) was taken on a tall hill (approximately 10 m high) and consists of a brownish-red ocher-like material. The second sample was taken about 10 m away from the first on the same hill.

The authors' affiliations are: R. Hekinian, Centre Océanologique de Bretagne, Brest Cédex 29273, France; M. Fevrier, Centre Océanologique de Bretagne and Université de Bretagne Occidentale, Brest Cédex 29200; J. L. Bischoff, U.S. Geological Survey, Menlo Park, California 94025; P. Picot, Bureau de Recherche Géologique et Minière, Orleans Cédex 45018; and W. C. Shanks, Department of Geology and Geophysics, University of Wisconsin, Madison 53706.

0036-8075/80/0328-1433$02.00/0

A small circular hole on the summit of one of these hills was noted and may be the main vent through which metal-bearing solutions were extruded (*7*). The third sample taken during dive Cy 78-08 was recovered from the middle hill and has a brownish-red surface with green patches (sample 8-14C).

Other small hills containing reddish and black material occur farther away on the top of a faulted wall. These hills have irregularly domed structures that may be hydrothermal vents. During another dive (Cy 78-06) in the same general area, a conical structure having a scoriaceous appearance was also observed on a sedimented bottom. The sediment surrounding the hills is made up of reddish-brown, yellowish-red, and dark gray friable material, which appears to result from the degradation of the conical hills. Small, bright yellow arborescent conelets (10 to 20 cm wide and a few centimeters high) were also noted in the vicinity of the columnar edifices. Basaltic glass recovered from the dispersed debris associated with sulfides shows no trace of secondary alteration. The types of structures and materials encountered in the polymetallic deposits are listed in Table 1.

Analytical Techniques

Minerals were identified by polarizing and metallographic microscopy and x-ray diffraction techniques. Bulk samples (Table 2) were chemically analyzed at the Centre de Recherches Pétrographiques et Géochimiques (CRPG) in Nancy and at the U.S. Geological Survey (USGS) in Menlo Park, California, by atomic absorption spectroscopy (Fe, Zn, Cu, As, and Pb), and optical emission spectroscopy (Si, Fe, Zn, Cu, Ag, Pb, Co, and Cd). Bulk samples were analyzed for Au and Pt by shortwave optical spectroscopy at the USGS.

Computerized electron microprobe analyses were carried out at the Centre Océanologique de Bretagne (Camebax de l'Ouest). During the analyses, the accelerating voltage was kept at 15.0 kilovolts. The electron beam incidence of the Camebax has a takeoff angle of about 42° and the limit of detection is about 500 parts per million (ppm). The precision of the method used is about 1 percent in the absolute value of concentration. Pure metals (99.99 percent) were used as standards to determine the concentrations of Cu, Ag, Au, and Pt. Samples of FeS_2, FeO, ZnS, and NiO were used to mea-

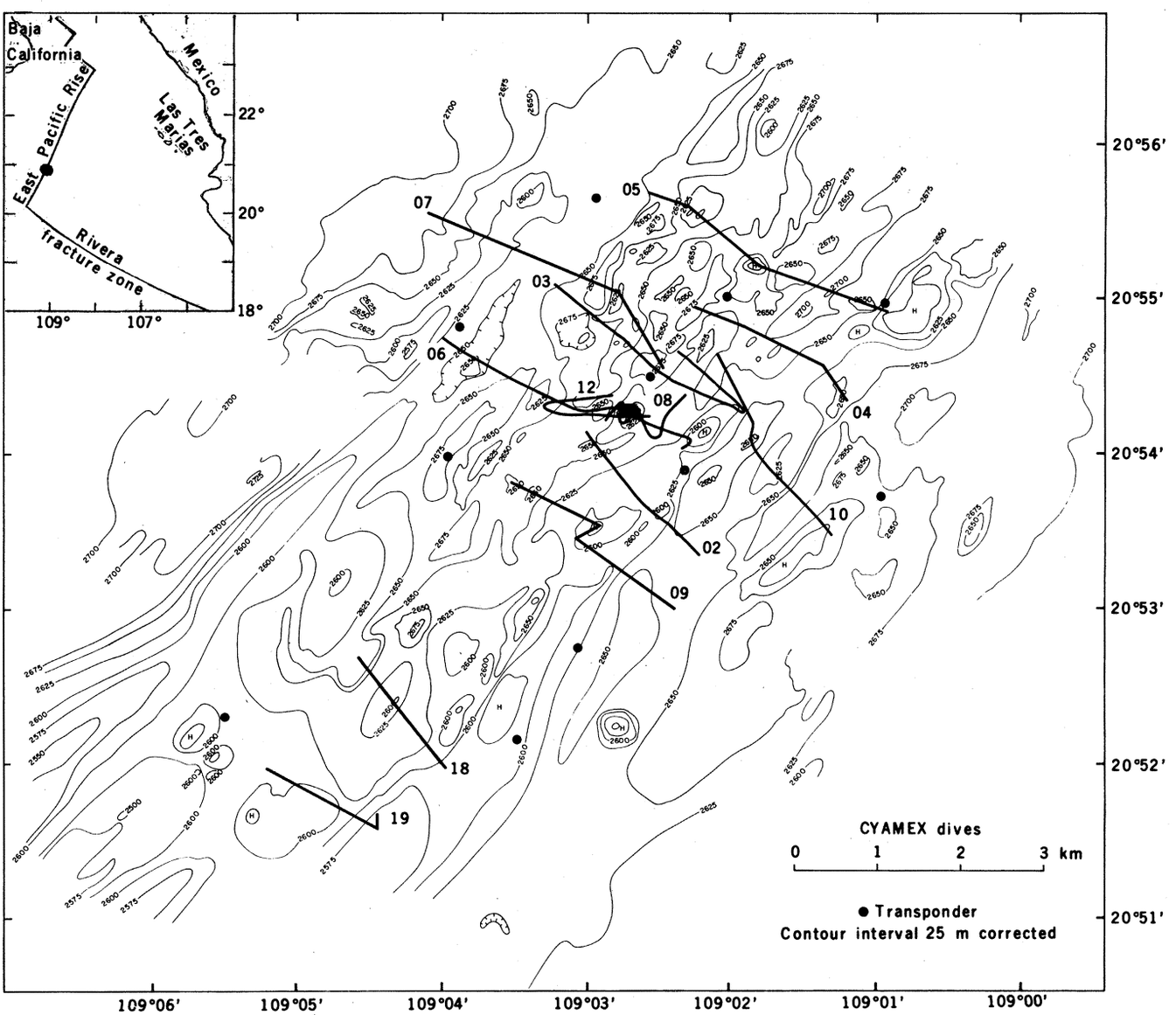

Fig. 1. Bathymetric map of the East Pacific Rise axial zone near 21°N (*24, 49*) showing the track lines of the *Cyana* dives and the area (blackened) where the massive sulfide deposits were discovered. (Inset) General map of the East Pacific Rise showing the location of the enlarged area.

sure the contents of S, Fe, Zn, and Ni, respectively.

The $K\alpha$ emission lines were used for the S, Fe, Cu, Zn, and Ni determinations; the $M\alpha$ emission lines for Au and Pt; and the $L\alpha$ emission lines for Ag. To avoid contamination, no silver compound was used as a conductor when analyzing for Ag. Other standard mineral compounds were used to determine the contents of the common oxides (SiO_2, Al_2O_3, FeO, MgO, MnO, CaO, Na_2O, and TiO_2). The bulk sample analyses were done by standard quantitative methods at the CRPG in Nancy and the USGS in Menlo Park.

Sulfur isotopic compositions were determined on three of the sulfide samples. Because of its fine-grained collomorphic nature, the sphalerite was separated from coexisting pyrite (or marcasite) by a chemical technique. Bulk samples were ground (< 100 mesh), homogenized, and reacted with 6*N* HCl at 60°C while purging with nitrogen gas. The H_2S liberated by the sphalerite reaction was precipitated as Ag_2S. The extraction was continued for 1/2 hour to 2 hours until no further H_2S was produced. X-ray diffraction analyses of the residues indicated that only pyrite or marcasite remained.

Pyrite or marcasite was dissolved and oxidized in aqua regia–bromine solution. The resulting sulfate was precipitated as $BaSO_4$ and then converted to Ag_2S after reduction with carbon at 1150°C.

Samples of Ag_2S from both extractions were then separately reacted with Cu_2O at 850°C to produce SO_2 gas. Isotope ratios in SO_2 were measured by mass spectrometer. The $\delta^{34}S$ values are expressed as per mil relative to Cañon Diablo troilite.

Results

Tubular structures. Most fragments recovered from the mounds appear to be circular interconnecting tubes ranging in diameter from about 0.5 mm to about 3 cm (Figs. 2 and 3). The walls of the tubes consist of thin concentric lamellae 0.10 to 1 mm thick (Figs. 2 and 3). The tube walls are composed of alternating lamellae of pyrite, hydrous amorphous silica, hydrous iron oxide, sphalerite, and wurtzite (samples 8-14A11, 8-14A2, and 12-40Aa). Some tubes contain lamellae of zinc-bearing phases without pyrite (12-38A12 and 12-40B). Others contain only pyrite and marcasite lamellae alternating with amorphous silica (12-38A12 and 12-40Aa). Sphalerite and pyrite lamellae line the walls of tubes that are close together within the same specimen (12-4A). However, zinc- and iron-rich phases within the same tube are segregated from each other and are occasionally separated by a band of amorphous silica (8-14A2).

The external tube walls also consist of crystalline pyrite and alternating lamellae of amorphous silica and hydrous iron oxides. The phases characterizing each lamella are defined by sharp boundaries. Small patches of Fe-Si nontronitic clay often occur at the contact with hydrous iron oxide and amorphous silica lamellae (8-14A2) (Fig. 3). In the least oxidized specimens, the amorphous silica phase is in direct contact with lamellae of pyrite-marcasite or zinc-rich phases. In moderately oxidized tubular samples, the amorphous silica bands are in direct contact with hydrous iron oxide associated with relics of pyritic material (8-18A2 and 12-38A).

The concave side of the tubes (Fig. 3) is made up of a collomorphic globular pyrite-marcasite association with a thin rim of hydrous iron oxide (12-40Aa, 12-38A12, 8-14C3, and 8-14A2). The inner part of the tubes within the most hydrated and oxidized deposits consists of alternating lamellae of globular geothite, amorphous silica, and hydrous iron oxide (8-14A1). Occasionally, a thin discontinuous band of Fe-Si clay occurs within the amorphous silica lamellae (8-14A1).

These tubes appear to be the result of two distinct processes. Some represent conduits through which hydrothermal fluids have percolated and deposited the concentric sulfide-oxide lamellae. The fluids probably continued to percolate through the small tubes after the main frame of the mound was built. Other tubes seem to be the result of worm burrowing. Worms of the class Vestimentifera found in the Galápagos hydrothermal area have a chitinous tube rang-

Table 1. General description of the polymetallic sulfides and hydrous iron oxide deposits collected from the East Pacific Rise near 21°N.

Sample Cyp 78	Weight (g)	Density (g/cm³)	Coexisting phases*	Type	Macroscopic description
8-14A1	12		Fe oxide, Si, clay, py, ma, cu, ba	Gossan	Purple and reddish-brown friable material with massive and tubular appearance
8-14A2	141	2.25	py, gel, Fe oxide, sp, wu, Si, clay	Sulfide	Dark gray massive with tubular structure
8-14A3	90.5		sp, gel, py		
8-14A11	1.2		sp, py, clay, Si		
8-14B	39.0		Fe oxide, clay	Gossan	Yellowish-brown and brownish-red friable material
8-14C3	14.0		Si, Fe oxide	Gossan	Light reddish-brown with dark gray streaks, friable material, traces of tubular structures
8-14C4	7.0		wu + gel, sp, py, Si	Sulfide	Dark gray with traces of light brown material, tubular structures with concentric lamellae
12-38A	7.8		py, Fe oxide	Sulfide	Dark gray sand-size fragments
12-38A4	11.3		cp, cu, di, py, sp	Sulfide	Dark gray fragments with green and yellow patches showing massive and tubular structures
12-38A6	6.2		py, Si, ma, sp, di		
12-38A7	13.8		cp, cu, di, Cu-py		
12-38A12	7.2		py, Cu-py, ma, Si, Fe oxide		
12-37	11.2		Fe oxide, Si	Gossan	Light reddish-brown debris of extremely friable material
12-40Aa	38.7	2.97	py, gel + wu, sp, Si, Fe oxide, ma, co	Sulfide	Dark gray compact sulfide fragments with tubular structure and reddish-brown zones
12-40B	90.7		py, sp, Si, Cu-py, ma, Fe oxide	Sulfide	Dark gray fragment of a tube, concave side lined with crystalline sulfides
12-40C5	4.6	—	py, sp, co, ma	Sulfide	Debris of dark gray material
12-41D	0.30		py, Cu-py	Sulfide sediment	Small debris of ocher material and fragment of basaltic glass

*Abbreviations are: Si, amorphous and hydrated silica; py, pyrite; sp, sphalerite; cp, chalcopyrite; cu, cubanite (high temperature); di, digenite; Cu-py, copper-bearing pyrite; ma, marcasite; Fe oxide, hydrated iron oxide; ba, barite; wu, wurtzite; gel, gel-like material.

Table 2. Bulk sample analyses of polymetallic sulfides. Analyses were done at the USGS and the CRPG (Nancy) by atomic absorption spectroscopy (for Fe, Zn, Cu, Ag, and Pb) or optical emission spectroscopy (for Si, Co, and Cd). Analyses of sulfur were done by gaseous phase chromatography (LECO). The values for silver shown in parentheses were measured on a separate portion of the sample.

Constituent	Amount of constituent in sample				
	8-14A2 (USGS)	8-14A2 (CRPG)	12-40Aa (USGS)	12-38A12 (USGS)	12-40B (CRPG)
	Percent by weight				
S	30.25	30.17	35.16	52.47	45.86
Cu	0.28	0.40	1.16	0.28	1.51
Fe	8.9	1.37	12.6	45.4	1.28
Zn	49.7	22.89	49.7	0.05	N.D.*
SiO_2	10.7	N.D.	2.14	0.1	N.D.
Total	99.83		98.62	98.16	
	Parts per million				
Ag	380	480	290 (121)	320 (145)	83
Pb	640	N.D.	330	520	N.D.
Cd	300	N.D.	700	< 70	N.D.
Co	< 10	N.D.	500	500	N.D.

*N.D., not detected.

ing from about 2.5 to 33.8 cm in diameter (*8*). The smallest known diameter for these worms is close to the observed diameter of the tubes in the East Pacific Rise deposits. Tubes that have contorted features rather than a more linear structure may be due to such a biogenic process. The fact that all the tubes recovered show concentric compositional arrangements suggests that they all served as pathways for fluid discharge.

Sulfides. Sulfide phases show well-developed cubes, tetrahedrons, spheroids, and triangular bipyramids as well as lath-like reniforms and globular textures. Pyrite and marcasite comprise about 50 percent of the bulk material, zinc sulfide about 34 percent, and copper-rich phases about 16 percent.

Pyrite occurs everywhere in the samples; it is found lining the walls of the tubular structures, as globular framboidal and reniform material, and as well-developed crystals forming the inner massive portion of the specimen. Trace constituents of pyrite include copper (0.1 to 0.2 percent) and zinc (0.3 percent) (Table 3 and Fig. 3).

Marcasite has strong pleochroism, varying from light brown to bluish-green, and it occurs as radiating laths forming individual globular structures (Fig. 4). The nuclei of those globules occasionally contain crystals of pyrite (12-A12). Other marcasite crystals occur in a fanlike arrangement with the tubular structures or along the inner massive portion of the sample (12-38A12 and 12-40B). The results of chemical analyses of marcasite are shown in Table 3 and do not differ from those of pyrite.

Pyrrhotite is a rare constituent of the sulfides and is difficult to identify because most of the mineral has been altered. Sometimes the massive pyrite and the marcasite show gray laths as inclusions or surrounding the crystals (12-38A12 and 12-41D), and these appear to be a replacement product. The microprobe data on these inclusions indicate about equal amounts of sulfur and iron (36 percent), copper (4 percent), and chloride (1.5 percent); other analyses of similar material (12-40B and 12-38Ab) show higher iron (> 46 percent) and lower sulfur (35 to 38 percent). None of the analyses of these laths add up to 100 percent, probably because of the hydrat-

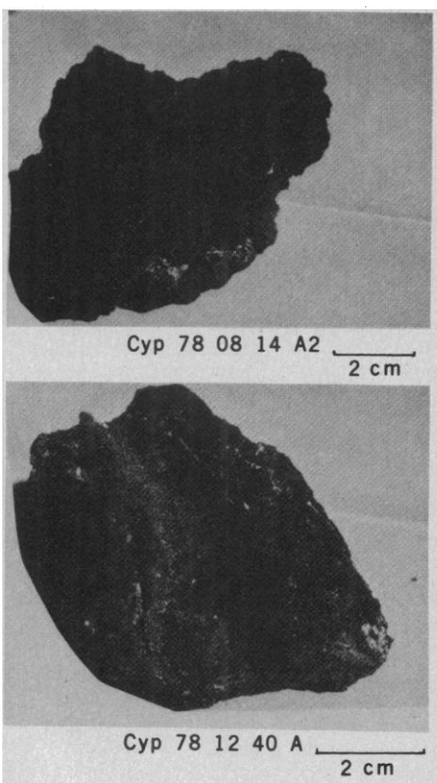

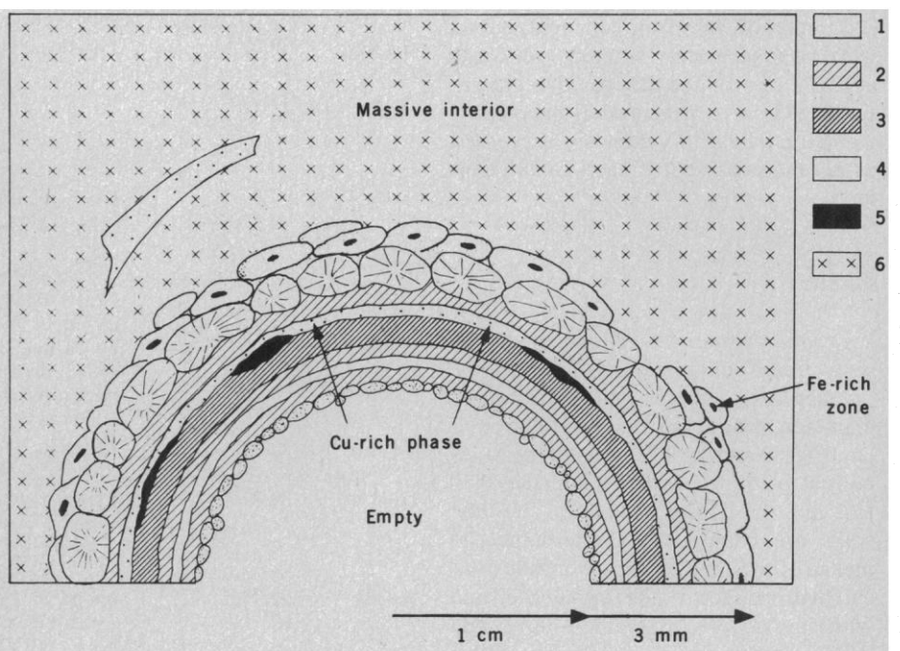

Fig. 2 (left). Fragment of polymetallic sulfide from the East Pacific Rise showing tubular structure. Sample Cyp 78-08-14A2 consists of pyrite, sphalerite, amorphous silica, and a moderate amount of hydrous iron oxide. Sample Cyp 78-12-40A is a fresher sulfide and has the concave part of the tube lined with massive pyrite. Fig. 3 (right). Sketch of hypothetical tubular structure in cross section showing different types of lamellae. Composition of the lamellae: 1, gel-like material having the composition of wurtzite; 2, crystalline pyrite or sphalerite, or both; 3, hydrous iron oxide; 4, amorphous silica; 5, pockets of Fe, Si-clay-rich material; and 6, massive crystalline interior of the samples, which is formed by sphalerite, pyrite, and chalcopyrite.

ed nature of the material. Chemical and mineralogical observations indicate that the laths are intermediate between a pyrrhotite and a mixture of pyrite and marcasite (*25*). Pyrrhotite is replaced by these intermediate products, and in only a few instances are small crystal residues observed as inclusions.

Copper-bearing pyrite is a term used here to describe metallic phases that are rich in both sulfur and iron but differ from normal pyrite in their higher copper content (2 to 10 percent) (Table 3). Copper-bearing pyrite, always accompanying normal pyrite, occurs in bands alternating with the concentric layers of pyrite forming botryoidal and framboidal structures (12-40B). Amorphous silica often forms the outer rims of these framboids (12-40B and 12-38A12).

Chalcopyrite was found in abundance in two samples (12-38A4 and 12-38A7) (Table 1). It occurred as yellowish massive crystals with abundant exsolution lamellae of chalcopyrrhotite and as a guest mineral in pyrite. Microprobe analyses show a composition of 29 to 33 per-

Table 3. Electron microprobe analyses of Fe-, Cu-, and Zn-rich sulfides from polymetallic deposits. Values are percentages by weight. The types of texture with which the sulfides are associated are shown. Concentrations less than 0.1 percent by weight are considered trace amounts (Tr). Gel-like material refers to wurtzite.

Constituent	Marcasite		Pyrite tube (N = 20)	Copper-bearing pyrite exsolution (N = 3)	Chalcopyrite (N = 7)	High-temperature cubanite massive interior (N = 9)	Digenite (N = 9)	Gel-like material		Sphalerite	
	Globular (N = 4)*	Tube (N = 5)						Tube (N = 7)	Massive (N = 17)	Tube (N = 7)	Massive (N = 17)
S	51.77	52.11	50.35	49.11	33.14	35.77	22.60	33.26	33.33	31.68	33.38
Cu	Tr	N.D.†	0.46	2.82	35.42	23.43	74.36	0.15	0.19	0.10	0.28
Fe	46.13	46.98	48.49	45.59	30.85	40.56	1.97	4.34	4.58	5.99	10.31
Zn	N.D.	N.D.	0.23	Tr	Tr	Tr	Tr	61.37	61.26	59.93	54.41
Ni	Tr	Tr	N.D.	N.D.	N.D.	Tr	N.D.	N.D.	N.D.	N.D.	N.D.
Ag	Tr	0.13	Tr	Tr	Tr	N.D.	Tr	N.D.	Tr	Tr	Tr
Au	0.79	0.40	Tr	Tr	Tr	N.D.	N.D.	Tr	Tr	Tr	Tr
Pt	0.55	0.28	N.D.	N.D.	0.10	Tr	Tr	N.D.	Tr	Tr	N.D.
Total	99.30	99.90	99.53	97.52	99.51	99.82	99.93	99.12	99.36	97.70	98.38

*Number of determinations used to obtain average shown. †N.D., not detected.

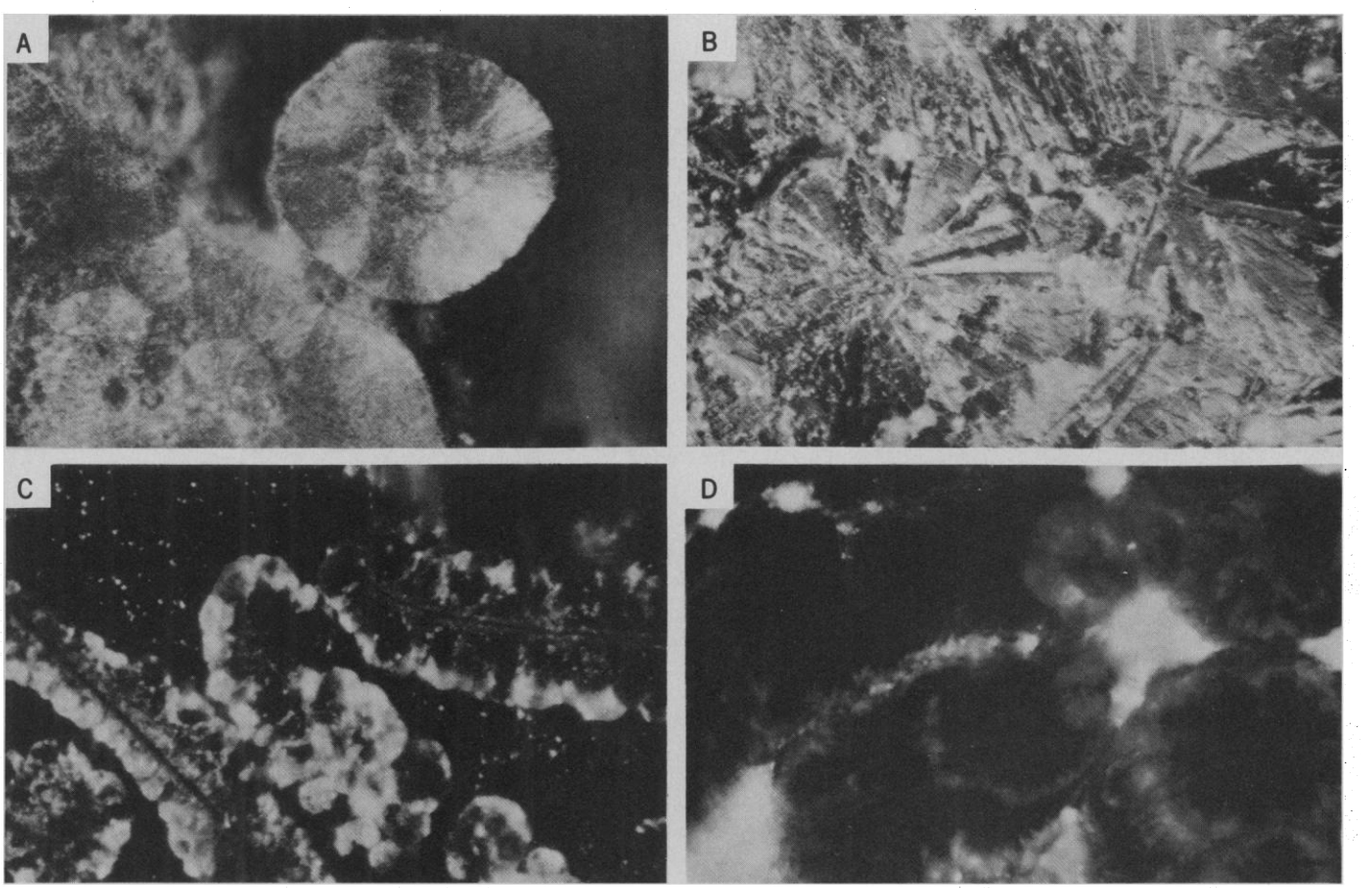

Fig. 4. Micrographs of polymetallic sulfides. (A) Framboidal pyrite under polarized light (sample 12-41D, ×170). (B) Spherulitic marcasite under polarized light (12-38A12, ×85). (C) Festoon-like structure of gel-like material having the composition of sphalerite. Linear textural features at the center of the agglomerate consist of crystalline pyrite inclusions (8-14A11, ×170). (D) Petal-like gel material showing variolitic textural features. Darker zones are made up of the iron-rich phase sphalerite (8-14C4, ×100).

cent copper, about 34 percent sulfur, and 32 to 36 percent iron (Table 3). Trace constituents associated with this mineral are cobalt (about 0.1 percent), zinc (0.1 percent), silver, and platinum. Dark pinkish areas with a higher copper content (45 to 68 percent) and lower sulfur (25 to 27 percent) and iron (7 to 23 percent) contents than chalcopyrite occur as inclusions in the chalcopyrite crystals. Sometimes chalcopyrite shows marginal replacement by digenite and covellite.

The ternary copper-iron-sulfur diagram of Kullerud (*26*) and Cabri (*27*) is used to illustrate the field of composition covered by chalcopyrite and associated copper-bearing minerals (Fig. 5). All the chalcopyrite minerals analyzed show a narrow range of composition close to that of cubanite (Fig. 5).

High-temperature cubanite occurs as small cubic crystals often as exsolution lamellae in the chalcopyrite (12-3A7). It was also noticed forming small massive patches, which were sometimes altered to a light brown material and included in the pyrite (12-41D and 12-38A4). X-ray powder diffraction of high-temperature cubanite shows the major intensity peaks at 3.062 and 1.876 angstroms. Both microscopic and x-ray diffraction studies indicate a high-temperature variety corresponding to the impure type of cubanite referred to by Ramdohr (*28*) as chalcopyrrhotite. High-temperature cubanite differs chemically from chalcopyrite by its higher iron (35 to 42 percent) and lower copper (25 to 29 percent) content (Table 3). Trace amounts of cobalt, zinc, and selenium were detected.

Digenite is an accessory constituent occurring as irregular inclusions and as reaction rims around chalcopyrite (12-38A7). Microprobe analyses indicate high copper (71 to 74 percent) and sulfur (22 to 25 percent) contents, a moderate amount of iron (2 to 6 percent), and trace amounts of silver (0.2 percent) and zinc (0.1 percent) (Table 3).

Small amounts of another copper-rich mineral intermediate in composition between chalcopyrite and digenite were detected as inclusions in chalcopyrite. This type of mineral falls close to the field of bornite in the ternary Cu-Fe-S diagram (Fig. 5). Tiny crystals of covellite were observed as inclusions in sphalerite (8-14A5) and marcasite (12-410).

Sphalerite is the second most abundant mineral after pyrite. The crystals are isotropic with reddish-pink internal reflections. Light and dark isotropic globular and reniform sphalerites are also common (Fig. 6). Sphalerite is found as inclusions in pyrite (12-38A12 and 12-405) and a host mineral for chalcopyrite ((8-14A3 and 12-38A4) (Table 3). The copper content is about 0.1 to 0.6 percent and the iron content 6 to 1 percent (Table 3). In some samples crystals of sphalerite are surrounded by a polygonal band of hydrous Fe,Si-rich material (8-14A4 and 8-14A11) which appears to be a late replacement product (Fig. 7). Chemical analyses show a relatively high zinc content (≃ 5 percent) compared to the other Fe-Si clay and iron-oxide compounds.

Wurtzite is a common constituent of the sulfide deposits and usually appears as yellowish-brown to reddish-yellow "gel-like material." Irregular globules, often agglutinated and showing festoon-like or petal-like forms, are seen (Fig. 4). Small pyrite crystals are found forming nuclei for the petal-like forms (8-14A2) (Fig. 4). Wurtzite commonly occurs as either flat hexagonal crystals or spherulites showing a black cross under the microscope. Incipient crystallization of sphalerite forms small intergrowths of radiating fibers in spherulitic wurtzite. Often, wurtzite is rimmed by late-crystallizing sphalerite.

Results of the microprobe analyses of wurtzite are fairly consistent with those of sphalerite, except that wurtzite has higher zinc (60 to 62 percent) and lower iron (3 to 5 percent) contents (Table 2). Often the wurtzite contains darker, more opaque zones that are enriched in iron compared to the lighter, yellowish-green zones. The difference in iron content between the two zones does not exceed 3 percent.

The distribution of FeS in the zinc-rich material shows three major peaks corresponding to different textures and assem-

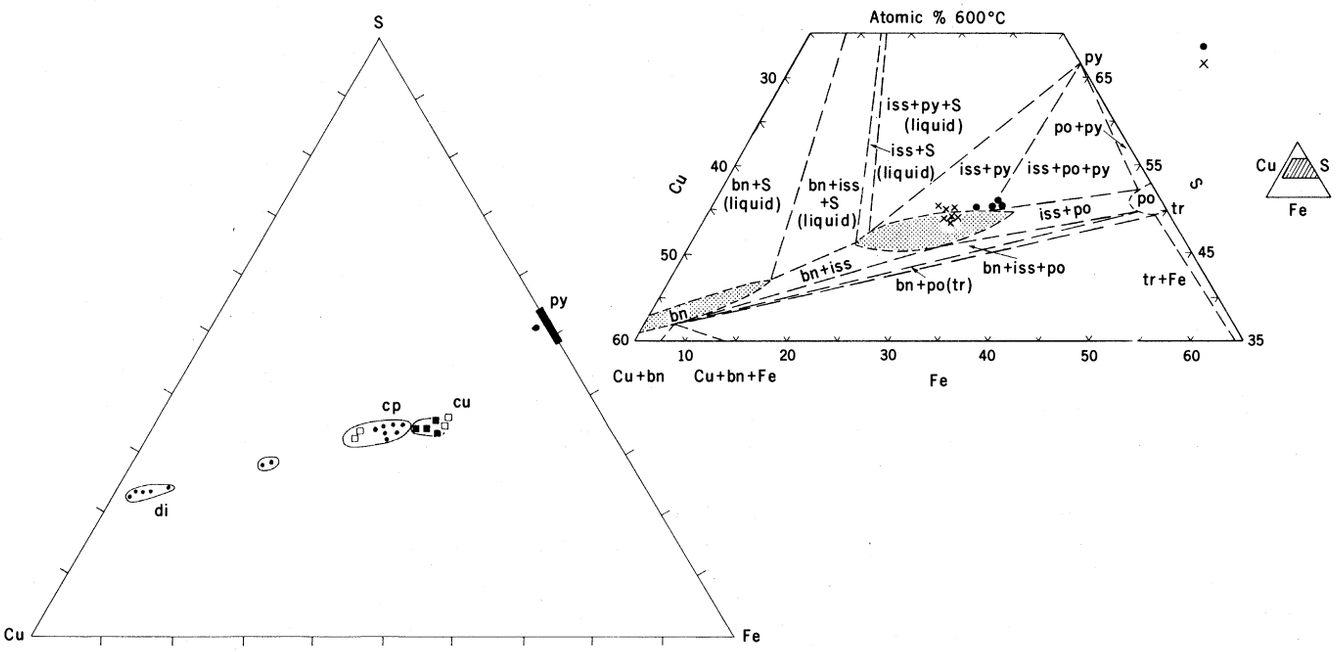

Fig. 5. Ternary diagram showing copper-rich phases (percent by weight) plotted on a restricted area representing various solid phases. Abbreviations: *di*, digenite; *cp*, chalcopyrite; *cu*, high-temperature cubanite; and *py*, pyrite. (Inset, on right) The 600°C isothermal diagram of Cabri (*27*) with fields of intermediate solid solution (*iss*). (•) High-temperature cubanite coexisting with chalcopyrite; (X) composition of chalcopyrite from this study; *bn*, bornite; *po*, pyrrhotite; and *tr*, troilite.

Table 4. Selected electron microprobe analyses of noble metal-bearing phases of polymetallic sulfide deposits. Values are percentages by weight. Gel refers to wurtzitic material.

Constituent	Silver-bearing phases				Gold-bearing phases				Platinium-bearing phases	
					Pyrite		Gel			
	Marcasite 12-38A12	Gel p-14A2	12-38A12 (N = 2)*	8-14A11	12-38A12	12-40Aa (N = 2)	12-40Aa (N = 2)	8-14A2 (N = 2)	Marcasite 12-38A12 (N = 2)	Chalcopyrite 12-38A7 (N = 2)
S	50.25	33.20	24.9	22.64	50.65	51.38	32.85	32.18	52.54	34.96
Cu	0.31	N.D.†	4.85	6.93	0.16	0.29	0.10	N.D.	N.D.	30.92
Fe	45.80	4.24	25.90	4.82	46.18	47.48	2.35	3.69	46.42	33.84
Zn	N.D.	61.77	N.D.	49.95	N.D.	N.D.	62.70	61.60	N.D.	N.D.
Ag	0.98	1.19	23.75	16.81	N.D.	N.D.	0.10	0.10	N.D.	0.20
Au	N.D.	0.79	0.40	N.D.	3.15	0.50	0.60	0.96	N.D.	N.D.
Pt	N.D.	0.68	N.D.	N.D.	N.D.	N.D.	N.D.	N.D.	1.17	0.32
Total	97.34	101.87		101.15	100.14	99.65	98.70	98.53	100.13	100.24

*Number of determinations. †Analyzed for but not detected.

blages. The average is about 6 mole percent FeS for the gel (wurtzite) (Fig. 8). Crystalline sphalerite associated with pyrite and chalcopyrite has an average of 15 mole percent FeS (Fig. 9). Sphalerite occurring as inclusions in pyrite has an average FeS content of 21 mole percent (Fig. 9).

Noble metals. High levels of silver (290 to 480 ppm) were found in the bulk sulfide samples (Table 2). These concentrations greatly exceed those in the Red Sea deposits (50 ppm) (*29*) and in oceanic basalts (1 to 2 parts per billion) (*30*). Although high levels of both gold and platinum were detected by microprobe, the contents in the bulk samples were below the detection limits (0.2 and 5 ppm, respectively). The detection limit for gold is well below its ore-grade level (5 to 10 ppm) but that for platinum is well above the ore-grade level (100 ppb), indicating the desirability of further platinum analyses.

Twelve samples analyzed by microprobe contain noble metals (Tables 3 and 4). However, only silver was present as a discrete mineral. Platy white silver-bearing minerals (10 to 60 micrometers in diameter) were detected by electron scanning microscopy and occur in pyrite (12-40B), sphalerite (12-40Aa), and copper-bearing pyrite (12-38A12) lining the tube walls (Fig. 10). Other silver grains occur within the massive portion of the samples set in a matrix of pyrite or chalcopyrite. They are surrounded by a rim of sphalerite, which in turn is included in a groundmass of pyrite (8-14A11). These samples contain variable amounts of silver (up to 36 percent), sulfur (1 to 23 percent), zinc (16 to 50 percent), copper (6 to 10 percent), and iron (4 to 38 percent) (Table 4). Microprobe analyses of several silver grains suggest a negative correlation between silver and copper contents (Fig. 11).

Silver was detected in pyrite, sphalerite, copper-bearing pyrite, marcasite, digenite, and gel-like material (12-40Aa, 12-38A, 12-38A12, 12-38A7, 8-14A2, and 8-14A11) (Table 4).

The concentration of gold in the various phases varies from 0.1 to 3 percent by weight. The highest concentration occurs in sphalerite and pyrite. Platinum was detected as a dispersed constituent

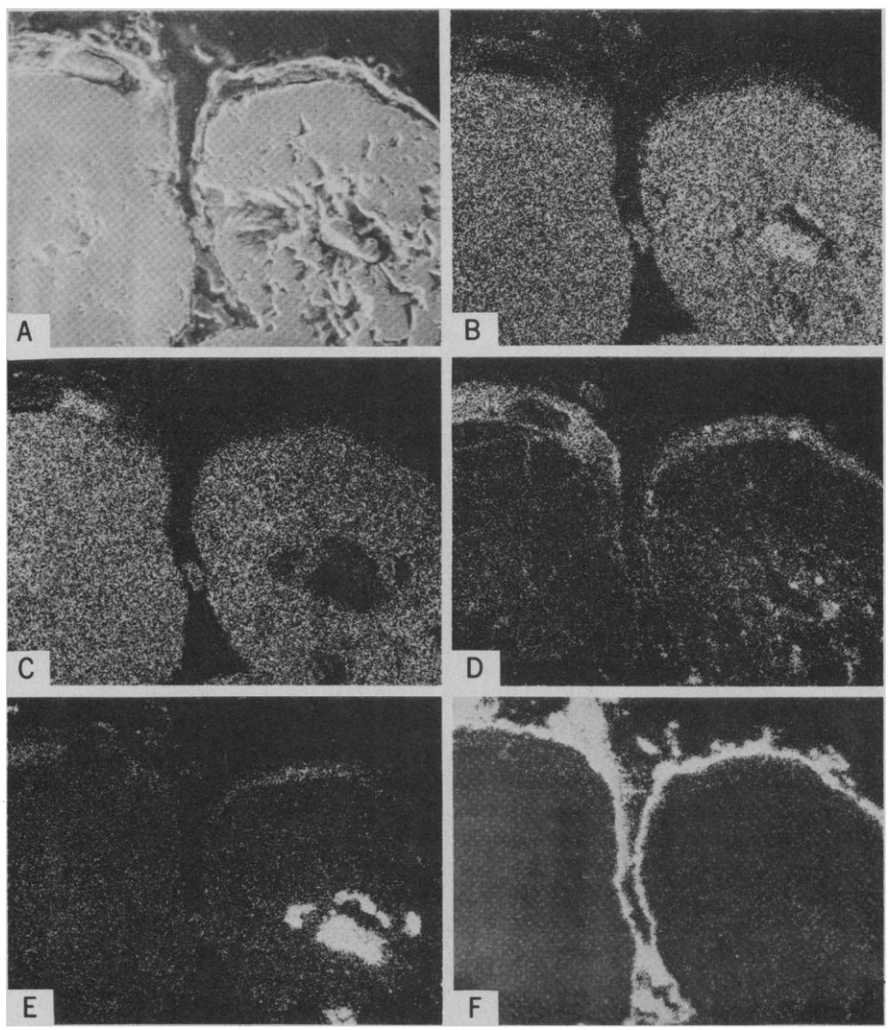

Fig. 6. Scanning electron micrographs of globular structure of sphalerite (sample 12-40Aa, ×225) with a pyrite forming the nucleus (A). The outer margin of the globule consists of a copper-rich phase surrounded by amorphous and hydrated silica. (B–F) The x-ray imaging of sulfur, zinc, copper, iron, and silica. The brighter zones relate with the major concentration of the element present.

in most sulfide phases that contain gold and silver; the platinum content in these phases varies between 0.1 and 1.4 percent by weight (Table 4).

Sulfates. The sulfates are common minor constituents of the deposits and are present as hydrated compounds with copper, iron, and zinc.

Copper-iron sulfates occur as laths that appear gray in reflected light and reddish-brown in refracted light. This type of material is found in samples composed primarily of pyrite and may represent an alteration product of chalcopyrite (12-41D and 12-40B). Chemical analyses of several laths show a decrease in the CuO content (from 14 to 2 percent) and an increase in the FeO content (from 29 to 71 percent). It appears that during hydration the iron was oxidized, copper and sulfur were subsequently lost from the compound, and a limonitic product was ultimately formed. Mineral phases such as copiapite and chalcanthite were identified by x-ray diffraction and microscopy (12-38A).

Zinc sulfates were identified in association with the other sulfates. White translucent fibers of melanterite and dark green anisotropic aggregates of goslarite were also detected.

Barite is a late mineral phase that occurs as radiating laths included in goethite and occasionally in marcasite. Some other sulfate phases identified were gypsum and jarosite.

Silicates. Siliceous material occurs in two distinct forms, as a hydrated amorphous silica and as a crystalline silicate phase.

Hydrated amorphous silica occurs as grayish-white bands less than 1 millimeter thick associated with polycrystalline sulfides and hydrous iron oxide. The bands coat the tube walls, form the outer rim of some pyritic globules (12-40B and 8-14C4), and occur in the massive portion of the samples. Many amorphous silica bands contain specks ($< 10\ \mu m$) of pyrite and copper-bearing pyrite (Fig. 3). Chemical analyses of amorphous silica show a high SiO_2 content (averaging about 88 percent) and minor amounts of Al_2O_3 (about 2 percent) (Table 5). Other constituents of the white bands include Na, K, Fe, Ca, and traces of Zn, S, Cu, and Ti (Table 5).

The crystalline silicate phases are common. Light green and light brown clay material of nontronitic composition is the most abundant silicate associated with amorphous silica bands and hydrous iron oxides. Microprobe and bulk analyses of hand-picked material indicate high silica (SiO_2, 17 to 68 percent) and iron (Fe_2O_3, 18 to 48 percent) and very low Al_2O_3 (0.1 to 2 percent) contents (Table 5). Other silicates include zeolite and muscovite which comprise less than 0.1 percent by volume of the bulk material. Muscovite up to 2 mm in diameter was found in one sample of massive sulfides (12-38A) and dispersed in sand- and clay-size material made up of intermixed sulfides, hydrous oxides, and basaltic glass. Microprobe analyses indicate a high K_2O content (11 to 12 percent) and low FeO and MgO contents (1 to 3 percent) (Table 5). A detrital origin of the muscovite flakes appears to be precluded by their angular shape, well-preserved outlines, and inclusion in the sulfides.

Hydrous iron oxides. Hydrated and highly oxidized material ("gossan") appears to be the low-temperature alteration product of the sulfides. Goethite and limonite are the most common iron oxides and have a powdery and friable appearance (Fig. 2). This material occurs as tiny globules showing concentric and radiating features varying in color from yellowish-red to ocher yellow. Hydrous iron oxides occur as alteration rims around crystals of sphalerite and pyrite (8-14A2) and as concentric bands lining the walls of the tubular structures (Fig. 3).

Chemical analyses show that the hydrous iron oxides consist primarily of Fe_2O_3 (61 to 72 percent), SiO_2 (3 to 10 percent), and S (1 to 9 percent), with a high water content (Table 5). Gradual replacement of sulfides by hydrated iron oxides is observed at the boundaries between the lamellae forming the tubes.

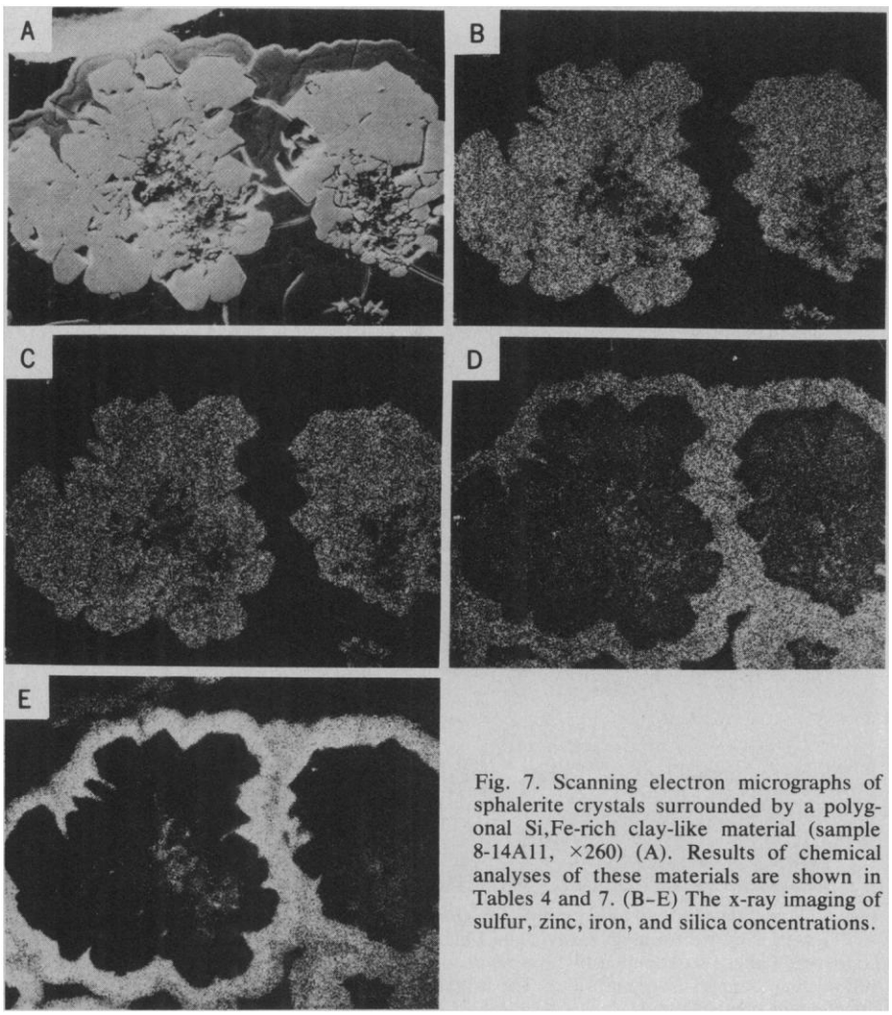

Fig. 7. Scanning electron micrographs of sphalerite crystals surrounded by a polygonal Si,Fe-rich clay-like material (sample 8-14A11, ×260) (A). Results of chemical analyses of these materials are shown in Tables 4 and 7. (B–E) The x-ray imaging of sulfur, zinc, iron, and silica concentrations.

Sea-Floor Alteration of the Sulfides

The lamellae found lining the tubes are alternating hydrous iron oxide–rich phases and sulfide phases. This compositional alternation could be due to the oxidizing conditions prevailing within a portion of the ascending solutions or to episodic precipitation of sulfide followed by oxidation.

The bulk altered specimens that form

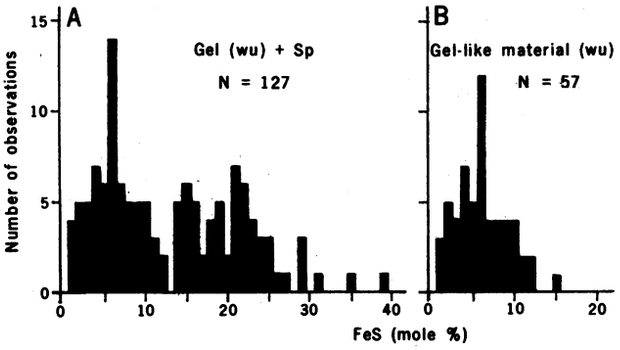

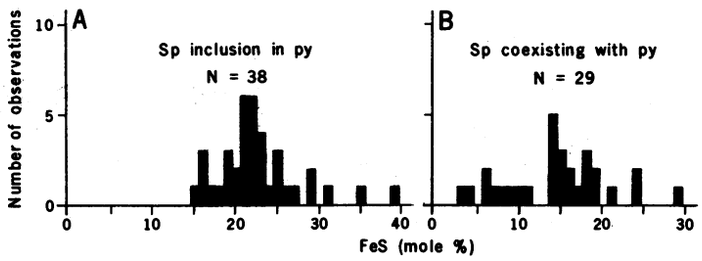

Fig. 8 (left). Frequency diagram of the FeS content in sphalerite (A) for all the samples analyzed and (B) for the gel-like material of wurtzitic composition. Fig. 9 (right). Frequency distribution of FeS content in (A) sphalerite (*Sp*) included in the massive pyrite (*py*) and (B) crystalline sphalerite coexisting with pyrite.

the gossans which comprise almost half of the total samples collected represent late hydrated and oxidized massive sulfides. Because of the highly oxygenated environment of deposition and the extremely fragile nature of the massive sulfides, most of the deposits lying on the accreting plate boundary of the East Pacific Rise will be altered, deteriorated, and dispersed in a relatively short period of geologic time. The sulfide deposits are likely to be preserved if they are buried by successive lava flows. However, in order to evaluate the degree of alteration of the various sulfide compounds it is important to make a detailed comparative study of active and inactive discharge zones.

Discussion

The sulfide deposits we studied constitute a fairly homogeneous material made up essentially of iron and zinc minerals followed by less abundant copper-rich phases. The possibility is not excluded that other types of deposits with different mineral proportions than those encountered at our sites could coexist within the same geological setting. The paragenesis of the massive sulfides from the East Pacific Rise indicates two major mineral assemblages: the association of chalcopyrite, high-temperature cubanite (chalcopyrrhotite), and pyrrhotite and the association of sphalerite and wurtzite. Pyrite and marcasite appear to be present with both types of mineral assemblages. In general, the chalcopyrite-cubanite-pyrrhotite association represents the initial phase of sulfide crystallization. This is suggested by the presence of chalcopyrite, sometimes observed as inclusions in sphalerite. Because of the poor preservation of the pyrrhotite in our samples it is difficult to interpret the genetic succession of this mineral. The sphalerite-wurtzite association is commonly found in the samples studied. Sometimes the wurtzite shows textural features rimmed by sphalerite, which suggest that it was formed before the sphalerite. Pyrite is often found as late precipitates surrounding sphalerite. The origins of the ocean floor sulfide deposits may be inferred by considering the geologic setting and some of the geochemical characteristics of the deposits.

Sulfur isotopes and source of sulfur. The sulfide may have originated from (i) reduction of seawater sulfate ($\delta^{34}S$ =

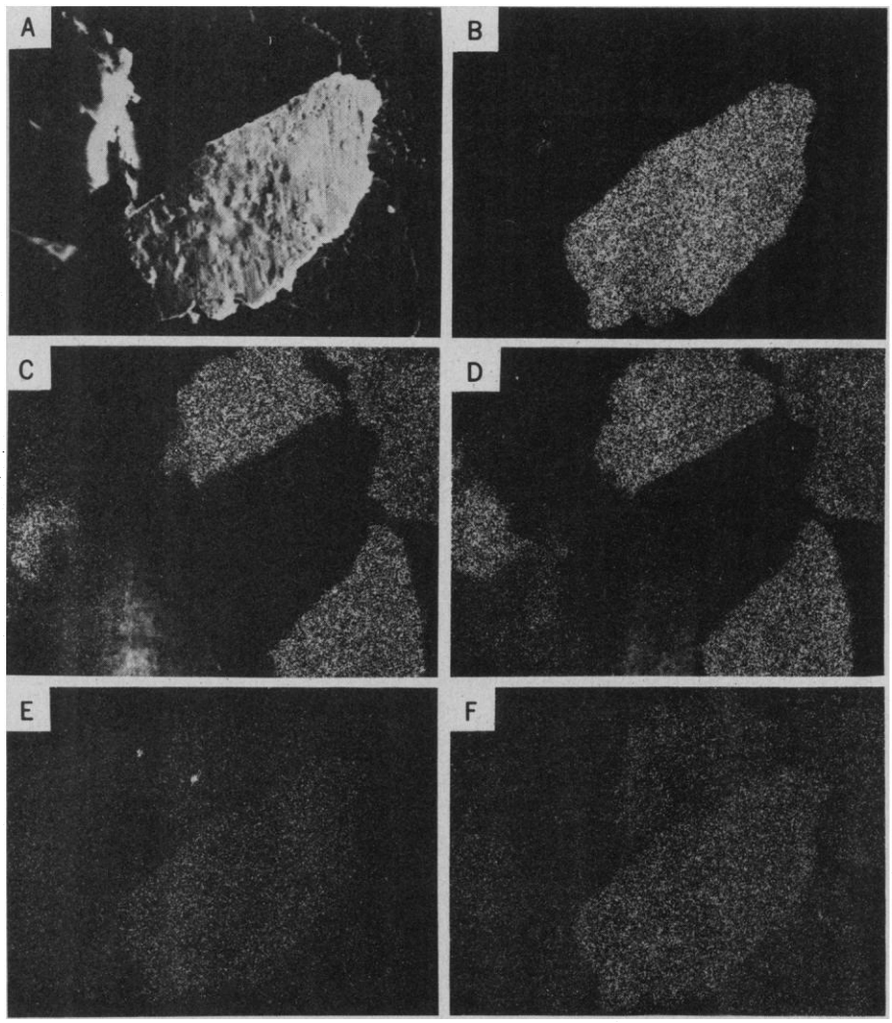

Fig. 10. Scanning electron micrograph of a silver grain (sample 12-40A, ×500) surrounded by massive pyrite (A). The time of sample exposition to the secondary electrons is 120 seconds. (B–F) The x-ray imaging of silver, sulfur, iron, selenium, and lead, respectively.

+ 20 per mil) during geothermal circulation of seawater, or (ii) mobilization of sulfide contained within the basaltic source material ($\delta^{34}S = 0 \pm 0.5$ per mil). Oceanic basalts have a sulfur content of 600 to 1800 ppm (*31, 32*), and some or all of this might be mobilized during interaction with heated seawater or other hydrothermal fluids. On the other hand, ferrous iron in basalt has the capacity to reduce seawater sulfates, provided the temperature of interaction exceeds about 300°C (*33*). Thus, sulfide could be mobilized from either source, or more likely a combination of both.

Measured $\delta^{34}S$ values of +1.9 to +3.3 per mil (Table 6) for the sulfides require that seawater sulfate is the source of at least some of the sulfur. A total of nine other isotopic analyses of pyrite, sphalerite, and chalcopyrite gave average $\delta^{34}S$ values of +3.45, +2.80, and +2.1 per mil, respectively (*33a*). If it is assumed that sulfate reduction is the exclusive source of the sulfide deposits, the isotopic fractionation between sulfate and H_2S is about +18 per mil (+20 to +2.4 per mil). Such a fractionation factor implies a temperature of 350°C if equilibrium is maintained (*34, 35*). At higher temperatures the fractionation becomes smaller, so admixtures of some magmatic sulfur would be required to obtain the observed $\delta^{34}S$ (Table 6). Thus, 350°C may be the lower limit of temperature for the production or mobilization of the sulfur.

Observed fractionation between coexisting pyrite and sphalerite is negligibly small (< 0.3 per mil; Table 6). This implies either that equilibrium occurred between these minerals at temperatures in excess of 600°C (*36*) or that fractionation did not occur because the minerals were deposited episodically at lower temperatures. The latter seems more likely, considering the observed mineral textures.

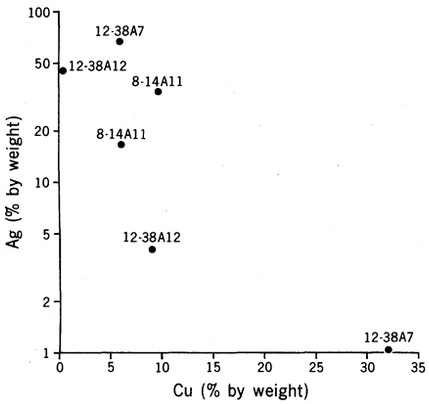

Fig. 11. Binary diagram of noble metal-bearing sulfide material.

Leaching and transport of preexisting basaltic rocks. Spooner and Fyfe (*37*), Parmentier and Spooner (*38*), and others have proposed convection systems involving the penetration and transport of seawater as a main mode of fluid circulation in the oceanic crust. During a seawater-basalt reaction, the seawater changes from a slightly alkaline solution containing chloride, sulfate, and sodium to a slightly acid solution containing sodium, calcium, and chloride (*39, 40*).

Mottl *et al.* (*33*) indicate that at higher temperatures (> 400°C) seawater might transport metals even under rock-dominated conditions. Thus, copper and zinc are likely to be leached from basaltic rocks at 300° to 400°C and form the appropriate sulfide phases when the hydrothermal fluid is cooled on the ocean floor.

Data on the mobility of heavy metals in altered ocean floor basalts showed that the concentration of zinc and copper in veins and veinlets is due to leaching during geothermal circulation (*41*). Massive sulfide deposits of the type found on the East Pacific Rise near 21°N might have been produced by a large volume of fluid trapped beneath the ridge axis. Also, large amounts of metal-bearing phases must have been dissolved from preexisting basaltic formations. For example, to produce a 3-m^3 mound containing 50 percent zinc, it would be necessary to leach about 15,000 m^3 of basalt with a zinc content of 100 ppm. We speculate that leaching of basaltic rocks in the vicinity of a shallow molten zone (< 2 km deep) could enhance the solubility of penetrating seawater in zones of extensive faulting and fissuring away from the ridge axis, where constructional features are more prominent. The heated seawater would leach the solidified basaltic material forming a roof over the completely or partially molten silicate (Fig. 12). Field observations (*21*) seem to indicate that sulfide segregation and precipitation coincide with a period of magmatic quiescence.

Hydrothermal fluid and magmatic segregates. Magmatic segregates including sulfur and other residual phases (metals and gas) that do not enter into the major mineral constituents of the basalt may be formed while a silicate melt is solidifying under the ridge axis. Several authors (*42–45*) have suggested that boiling solutions in vapor-dominated hydrothermal systems give rise to ore deposition at a relatively shallow depth in the crust. Heated seawater circulating near the surface (< 2 km), could interact with magmatic residual phases and facilitate the extrusion of the metal-rich solution onto the ocean floor. In this case, reduction of sulfates from fluid solutions (evolved seawater) could contribute to the production of sulfur with the $\delta^{34}S$ values observed (Table 6).

An alternative hypothesis is that of segregation of a sulfide melt from a purely magmatic source. The process involved in segregating a sulfide melt may be analogous to that known as the "filter-pressing phenomenon" (*46*) in which the immiscible or residual melts are expelled during the crystallization of a silicate magma. After the solidification of the major mineral phases (such as pyrox-

Table 5. Electron microprobe analyses of hydrous silica-bearing and iron oxide phases from polymetallic deposits. Values are percentages by weight. Total iron was calculated as Fe_2O_3 except for the muscovite sample and the bulk sample analyses. Concentrations less than 0.1 percent were reported as trace amounts (Tr). The type of textural association is indicated. The H_2O content was not determined. Ign, ignition loss.

Constituent	Amorphous silica tube (N = 12)	Clay tube	Clay* rim (N = 5)	Muscovite massive (N = 2)	Iron oxide tube (N = 8)	Gossan bulk	Gossan bulk	Gossan bulk
SiO_2	89.43	67.85	39.72	46.49	8.83	3.21	12.56	17.98
Al_2O_3	1.91	N.D.†	0.57	32.80	0.20	0.09	1.06	0.35
Fe_2O_3	0.40	19.81	28.25	N.S.	72.68	68.20	58.91	42.06
FeO	N.S.‡	N.S.	N.S.	2.22	N.S.	N.S.	0.71	0.03
MnO	Tr	Tr	N.D.	N.D.	Tr	N.D.	N.D.	N.D.
MgO	N.D.	0.17	0.45	1.45	Tr	0.09	0.79	1.06
CaO	0.20	0.13	0.37	N.D.	Tr	0.07	1.19	1.62
Na_2O	0.10	N.D.	1.30	0.30	Tr	Tr	N.S.	N.S.
K_2O	Tr	N.D.	1.07	11.24	N.D.	Tr	0.28	0.24
TiO_2	N.D.	N.D.	N.D.	0.70	Tr	Tr	Tr	Tr
PO_5	N.D.	N.D.	N.D.	N.D.	N.D.	N.S.	3.25	2.22
S^2	Tr	Tr	0.13	N.S.	1.78	N.S.	2.77	0.76
Cu	Tr	N.D.	Tr	N.S.	N.D.	N.S.	N.D.	N.S.
Zn	N.S.	N.D.	5.14	N.S.	N.S.	N.S.	N.S.	N.S.
Ign	N.S.	N.S.	N.S.	N.S.	N.S.	16.9	16.71	29.89

*This sample represents average analyses of Si,Fe-rich clay-like material surrounding rim of sphalerite (Fig. 8). †Analyzed for but not detected. ‡Not sought.

ene, plagioclase, and iron and titanium oxides) from a silicate magma, the solubility of sulfur in the magma would decrease and sulfide melts could separate. Only a small part of the sulfide melt might be incorporated in the silicate melt, and similarly the sulfide melt might trap only small amounts of the low-temperature silicate assemblages. Experimental studies by Mysen and Popp (*47*) showed that the solubility of sulfur in melts of diopsidic and albitic composition increases with pressure and temperature and suggested that most of the immiscible sulfide melt separated before the silicate melt reached the surface. The maximum temperature at which stoichiometrically pure pyrite and sphalerite will crystallize from a melt (about 800° to 1000°C) is lower than that of the basaltic minerals (1050° to 1200°C). Thus, a sulfide melt segregating from a silicate melt could enter cracks and fissures on the ocean floor or accumulate in pockets near a magma chamber.

The later hypothesis, that the sulfide deposits originated in a magmatic segregation process, has to be considered with reservations. The high content of zinc-rich phases in these deposits does not correspond to the composition of natural sulfides found trapped in ocean floor basalts. Indeed, several sulfide globules found in basaltic glasses associated with the deposits completely lack zinc, but have abundant sulfur (33 to 37 percent), iron (50 to 56 percent), nickel (6 to 9 percent), and copper (0.1 to 6 percent). Furthermore, it has been shown (*48*) that tholeiitic basalts contain sulfides with $\delta^{34}S$ values of +1.1 to −3.0 per mil, compared to the range of +1.9 to +3.3 per mil in the East Pacific Rise samples. To increase $\delta^{34}S$ to the average value of +2.5 per mil found in the samples studied, it would be necessary to have an admixture of sulfide from another source during the segregation of sulfides. The process most likely to have given rise to the sulfides described here is reduction of seawater sulfates at high temperatures.

Whether the massive sulfides and associated products from the East Pacific Rise are derived from leaching of preexisting basaltic rocks or interaction of heated seawater and magmatic segregates has not yet been established. The relation between sulfide and silicate melts in an oceanic environment is poorly defined. Many factors that control the separation of sulfur and other residual phases from silicate magmas are unknown. Also, experimental work on rock leaching and seawater transport at high temperatures is needed to provide a better insight into hydrothermal systems above 350°C. In addition, the tectonic setting associated with the preferential accumulation of sulfides in some regions rather than others is not well understood. Detailed studies of oceanic accreting plate boundaries are limited and comparative studies are rather speculative.

Table 6. Sulfur isotopic composition of sulfide minerals. Values are relative to Cañon Diablo troilite.

Sample	Mineral	$\delta^{34}S$ (per mil)
8-14A2	Sphalerite	+2.46, +2.91
	Pyrite	+2.33, +2.52
12-38A	Pyrite	+3.27
12-40A	Sphalerite	+1.87
	Pyrite	+2.01

Conclusions

The massive sulfide deposits found on the East Pacific Rise near 21°N form roughly conical and columnar structures of variable size (3 to 10 m in height) aligned approximately parallel to the axis of the accreting plate boundary (*17*). Lack of pelagic intercalated sediment indicates that these structures were built rapidly by direct discharge onto the ocean floor. The surrounding sand-sized material covering the basaltic flows is made up of polymetallic sulfide debris and associated assemblages deposited during discharge. The debris could also have been formed in part by degradation of preexisting vents.

Tubular structural features encountered on the sulfide edifices are small conelets (up to 5 cm in diameter) resulting from successive fumarolic exhalations. Many of the tubular structures are contorted and remind one of holes left by burrowing animals. The alternating composition of the lamellae lining the walls of the tubes suggests fractional precipitation of low-temperature assemblages (silica, iron oxides, clay-like material) and higher temperature sulfide phases (pyrite, sphalerite, chalcopyrite).

The major sulfide constituents are pyrite, marcasite, zinc-rich material, and copper-rich phases. The intimate association of pyrite and sphalerite suggests that both phases were formed in the same temperature range. The high-temperature cubanite and digenite formed as reaction rims, as exsolution lamellae, and as patches in chalcopyrite are probably the result of rapid crystallization. Assemblages of chalcopyrite and high-temperature cubanite probably represent the early phase of crystallization, before that of sphalerite and pyrite.

A gel-like material having the composition of wurtzite occurs throughout the samples. This material is believed to have been formed by rapid cooling at the sea floor–seawater interface. Many of the hydrous iron oxides (gossans) ob-

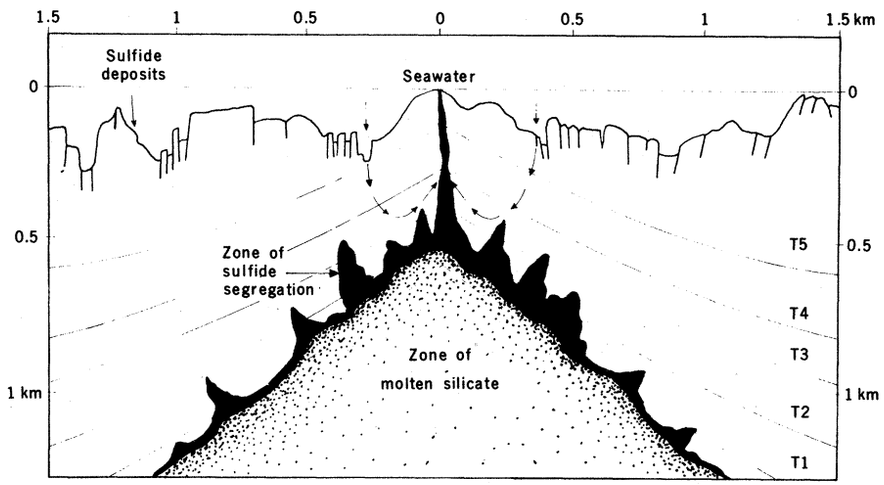

Fig. 12. Schematic representation of the axial zone of a rapidly spreading ridge system. The hypothetical zone of molten material has the composition of a basaltic melt capped by a zone of crystal-liquid segregation of sulfide and high-temperature solutions. Block-faulted areas are preferential sites for seawater fluid circulation system. Superimposed temperatures curves (*T*) are the calculations of Sleep (*50*) for a ridge spreading at a half-rate of 5 cm/year. Since the rate of spreading near 21°N is around 3 cm/year, the isotherms will be steeper and the top of the molten zone 1 to 2 km deeper in the crust than shown. Temperatures: *T1*, 1185°C; *T2*, 1000°C; *T3*, 800°C; *T4*, 600°C; and *T5*, 300°C. The bottom topography shown on the zero-line reference level is a composite profile made during *Cyana* dives Cy 78-06 and Cy 78-10 in the general area of the sulfide deposits. Vertical exaggeration of the bottom profile is two. The zone of molten silicate representing a magma chamber has no vertical exaggeration.

served forming large portions of the specimens collected, or replacing crystals of sulfides, result from low-temperature alteration of preexisting sulfide phases.

The principal silicates are hydrated amorphous silica and iron-silicon nontronite. Minor amounts of muscovite and zeolite were scattered throughout the samples. The sulfates consist mainly of Cu,Fe- and Zn-bearing phases. Small amounts of barite were also detected.

The sulfide deposits described here were probably formed in the axial part of the East Pacific Rise near 21°N during a period of magmatic quiescence. The nature of the polymetallic sulfides, the structural setting of the deposits, and the sulfur isotopic data suggest that they had a magmatic source. The massive sulfide deposits were probably formed by mobilization of sulfide-bearing material and by some reduction of seawater sulfates during fluid circulation in the oceanic crust. Whether the sulfide-bearing material was extracted from basaltic rocks or represents a sulfide melt segregated during the solidification of a silicate melt under the axis of the East Pacific Rise is not yet known.

References and Notes

1. K. Bostrom and M. N. A. Peterson, *Econ. Geol.* **61**, 1258 (1966).
2. Scientific Party, Leg 54, *Geotimes* **22** (No. 11), 19 (1977).
3. R. Hekinian *et al.*, *Oceanol. Acta* **1** (No. 4), 473 (1978).
4. R. B. Scott, P. A. Rona, L. W. Butler, A. J. Nalwalk, M. R. Scott, *Nature (London) Phys. Sci.* **239**, 77 (1972).
5. P. A. Rona, *Mar. Geol.* **21**, M59 (1976).
6. M. Hoffert *et al.*, *Oceanol. Acta* **1** (No. 1), 73 (1978).
7. J. R. Cann, C. K. Winter, R. G. Pritchard, *Mineral. Mag.* **41**, 193 (1977).
8. J. B. Corliss *et al.*, *Science* **203**, 1073 (1979).
9. G. Constantinou and G. J. S. Govett, *Inst. Min. Metall. Trans.* **81**, 1334 (1972).
10. _____, *Econ. Geol.* **68**, 848 (1974).
11. R. H. Sillitoe, *ibid.*, p. 1321.
12. R. W. Hutchinson and D. L. Searle, *Soc. Min. Geol. Jpn.* **3**, 198 (1971).
13. J. D. Smewing, K. O. Simonian, J. G. Gass, *Contrib. Mineral. Petrol.* **51**, 49 (1975).
14. E. H. Bailey and R. G. Coleman, *Geol. Soc. Am. Abstr. Programs* **7** (part 3), 293 (1975).
15. N. A. Duke and R. W. Hutchinson, *Can. J. Earth Sci.* **11**, 59 (1974).
16. R. G. Coleman, *Ophiolites* (Springer-Verlag, Berlin, 1977).
17. J. Francheteau *et al.*, *Nature (London)* **227**, 523 (1979).
18. R. L. Larson, H. W. Menard, S. M. Smith, *Science* **161**, 781 (1968).
19. K. Crane and W. R. Normark, *J. Geophys. Res.* **82**, 5336 (1977).
20. K. C. Macdonald and F. H. Spiess, *Eos* **60**, 376 (1979).
21. F. N. Spiess *et al.* (RISE Project Team), *Science* **207**, 1421 (1980).
22. M. Solomon and J. L. Walshe, *Econ. Geol.* **74**, 797 (1979).
23. CYAMEX Scientific Team, *Eos* **59**, 1198 (1978).
24. _____, *Mar. Geophys. Res.*, in press.
25. P. Picot and Z. Johan, *Atlas des minéraux métalliques* (BRGM, Paris, 1977).
26. G. Kullerud, *Fortschr. Mineral.* **41**, 221 (1964).
27. L. J. Cabri, *Econ. Geol.* **68**, 443 (1973).
28. P. Ramdohr, *The Ore Minerals and Their Intergrowths* (Pergamon, Oxford, 1969).
29. J. L. Bischoff and F. F. Manheim, in *Hot Brines and Recent Heavy Metal Deposits in the Red Sea*, E. T. Degens and D. A. Ross, Eds. (Springer-Verlag, New York, 1969).
30. D. Gottfried and L. P. Greenland, 24th. *Int. Geol. Congr.* (1972), sect. 10, p. 135.
31. J. G. Moore and B. P. Fabbi, *Contrib. Mineral. Petrol.* **33**, 118 (1971).
32. G. K. Czamanske and J. G. Moore, *Geol. Soc. Am. Bull.* **88**, 587 (1977).
33. M. J. Mottl, H. D. Holland, R. F. Corr, *Geochim. Cosmochim. Acta* **43**, 869 (1979).
33a. P. Picot and M. Fevrier, in preparation.
34. B. W. Robinson, *Earth Planet. Sci. Lett.* **18**, 443 (1973).
35. H. Sakai, *Geochem. J.* **2**, 29 (1968).
36. Y. Kajiwara and H. R. Krause, *Can. J. Earth. Sci.* **8**, 1397 (1971).
37. E. T. C. Spooner and W. S. Fyfe, *Contrib. Mineral. Petrol.* **42**, 287 (1973).
38. E. M. Parmentier and E. T. C. Spooner, *Earth. Planet. Sci. Lett.* **40**, 33 (1978).
39. J. L. Bischoff and F. W. Dickson, *ibid.* **25**, 385 (1975).
40. J. L. Bischoff and W. E. Seyfried, *Am. J. Sci.* **278**, 838 (1978).
41. S. E. Humphris and G. T. Thompson, *Geochim. Cosmochim. Acta* **44**, 127 (1978).
42. D. E. White, L. J. P. Muffer, A. H. Truesdall, *Econ. Geol.* **66**, 75 (1971).
43. W. S. Phillips, *Inst. Min. Metall. Trans.* **82**, 90 (1973).
44. L. M. Cathles, *Kennecott Copper Corp. Tech. Rep. 90-443* (1976).
45. C. H. Sondergeld and D. L. Turcotte, *Econ. Geol.* **74**, 109 (1979).
46. R. A. Daly, *Igneous Rocks and the Depth of the Earth* (McGraw-Hill, New York, 1933).
47. B. O. Mysen and R. K. Popp, *Carnegie Inst. Washington Yearb.* **77**, 709 (1978).
48. A. Schneider, *Contrib. Mineral. Petrol.* **25**, 95 (1970).
49. W. R. Normark, T. R. Alpha, G. R. Fess, G. S. Lichtman, C. E. Gutmacher, *U.S. Geol. Surv. Open-File Rep. 78-350* (1978).
50. N. H. Sleep, *J. Geophys. Res.* **80**, 4037 (1975).

51. We thank the scientific and technical teams who participated in the expedition CYAMEX for providing the samples studied here. The expedition was funded by the Center for the Exploitation of the Oceans (CNEXO) with contributions from the National Science Foundation, the U.S. Geological Survey, Woods Hole Oceanographic Institution, and the National Geographic Society. We are thankful to J. Francheteau for his encouragement. We are particularly grateful to M. Bohn, whose technical capabilities helped considerably in performing the electron microprobe analyses (Camebax) on our samples. We also thank G. Floch and D. Gueant for preparing the samples for microscopic examination, and F. Pillard and E. Oudin for help in the microscopic examination of some polished sections. We thank H. D. Holland and R. Koski for their constructive comments.